Tuning the photocatalytic activity of titanium dioxide by encapsulation inside zeolites exemplified by the cases of thianthrene photooxygenation and horseradish peroxidase photodeactivation

Gonzalo Cosa,[a] María S. Galletero,[b] Lorenzo Fernández,[b] Francisco Márquez,[b] Hermenegildo García*[b] and J. C. Scaiano*[a]

[a] *Department of Chemistry, Centre for Catalysis Research and Innovation, University of Ottawa, Ottawa ONKIN 6N5, Canada*

[b] *Instituto de Tecnología Química CSIC-UPV, Universidad Politécnica de Valencia, Apartado 22012, 46071-Valencia, Spain. E-mail: hgarcia@qim.upv.es*

Received (in montpellier, France) 7th February 2002, Accepted 29th April 2002
First published as an Advance Article on the web 16th September 2002

A series of Y, Beta, mordenite and ZSM-5 zeolites containing different amounts of nanosized TiO_2 clusters have been prepared by $Ti{=}O^{2+}$ exchange followed by condensation. The presence of $Ti{=}O^{2+}$ and its subsequent oligomerization can be followed in Raman spectroscopy by the appearance of the band at *ca.* 530 cm^{-1} and its replacement by others at 394, 460 and 637 nm. X-ray diffractograms of the solids show a considerable intensity decrease as the amount of TiO_2 present increases. High-resolution transmission electron microscopy (HRTEM) shows that no isolated TiO_2 particles are present in the case of zeolite Y, while the sample of mordenite at the highest Ti loading contains isolated TiO_2 particles distinguishable by HRTEM. Diffuse reflectance UV-Vis spectroscopy indicates that the bandgap and the apparent extinction coefficient depend remarkably on the Ti content as well as on the zeolite crystal structure. Quantum chemical calculations at the semiempirical level also predict large variations in the HOMO–LUMO energies as a function of the number of Ti atoms. It has been found that the photoactivity of TiO_2@Y and TiO_2@mordenite is higher than that of commercial anatase for the photooxygenation of thianthrene to thianthrene oxide ($\lambda_{ex} > 200$ nm), but smaller for the hoseradish peroxidase photodeactivation in aqueous buffer ($\lambda_{ex} = 350$ nm). These variations in the photocatalytic activity of TiO_2 illustrate the potential that inclusion of TiO_2 nanoclusters within zeolites has to modulate its photoactivity.

TiO_2 is by far the most important semiconductor that finds wide application as a photocatalyst for the degradation of pollutants,[1–22] in systems for the photochemical splitting of water[23–26] and in photovoltaic solar cells.[27–36] There is an enormous potential in controlling some of the photophysical and photochemical properties of bulk TiO_2 such as the onset of the absorption band related to the semiconductor bandgap and the efficiency and lifetime of photoinduced electron transfer processes. To achieve this control, a reduction of the particle size down to the nanometer range in which *quantum size effects* may operate has been pursued.[37–41] Nanoparticles of TiO_2 have been reported to exhibit distinctive properties, different from those characteristic of bulk TiO_2 particles.[37,42–44] However, this strategy is complicated by the instability inherent to nanoparticles and the tendency of the primary nanoparticles to undergo aggregation at neutral pH into grains of much larger size with a non-uniform distribution and to age changing the properties over the time.[42]

A novel approach that should lead to the control of the TiO_2 photoactivity and may help to circumvent the aggregation problem consists in the encapsulation of TiO_2 nanoclusters inside the rigid internal voids of zeolites that are on the nanometer scale.[45–59] This strategy offers a simple way to control the size, geometry and accessibility of the TiO_2 clusters by choosing among the known zeolites those with the appropriate pore dimension and topology.[60–62] In addition, the compartmentalized space defined by the zeolite framework would allow the design of a multi-component photochemical system comprising as part of it TiO_2 particles assembled inside the zeolite voids.[63,64] However, in spite of the promising advantages of the use of zeolites as organized media, the number of studies on the photoactivity of TiO_2 incorporated inside the pores of zeolites is still relatively small. Previous reports are limited to studies on the emission of zeolite-bound TiO_2,[65] intrazeolite electron transfer from TiO_2 to methyl viologen[50] and the photocatalytic activity of these materials for the decomposition of NO_x and the photoreduction of CO_2 by H_2O.[46,47]

The incorporation of TiO_2 clusters into zeolites should allow one to prepare photocatalysts with a range of distinctive activities. A range of variability in turn offers versatility and is a powerful tool to adjust properties to accommodate diverse needs in the catalysis and sunscreen fields. In this contribution we present two examples in which we have materialized the potential of zeolites to alter the photocatalytic activity of bulk TiO_2 in an advantageous way: in one case by increasing it, and in the other one by reducing the photoactivity of TiO_2 towards a biological target. In each of these cases the result is a desirable outcome of the modifications of the material; in other words, while opposite changes are obtained in the two examples, the material can be regarded as having in both cases improved properties for specific applications. For example, in the case of heterocyclic photooxygenation an increased activity represents an advantage giving rise to higher product yield. In contrast, in applications related to the use of TiO_2 in cosmetics, specifically sunscreens, a decreased photochemical reactivity towards biological targets represents a significant improvement, since ideally those materials should offer ultraviolet protection with no "side effects", such as damage to

 DOI: 10.1039/b201397e

tissues, or any other form of phototoxic or photoallergenic reactions. In this regard a strategy that has been followed to vary the photocatalytic activity of TiO_2 consists in the reduction of the TiO_2 particle size and coverage with an inert insulator.[66–69] In essence, this strategy to devoid TiO_2 particles of photocatalytic activity in the UV-A region is similar to what is described here.

The subject of this work are a series of TiO_2@zeolite samples in which the TiO_2 loading has been varied in zeolites of different pore sizes and topologies. The distinct catalytic activity mentioned above is a reflection of the control of the TiO_2 photochemical properties as result of the formation of clusters embedded within the zeolite micropores. This is manifested in a variation of the semiconductor's apparent extinction coefficient and effective bandgap.

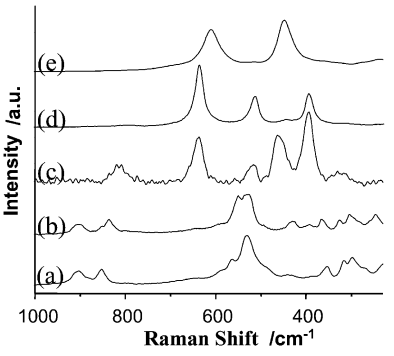

Fig. 1 Raman spectra of $(Ti{=}O)K_2(C_2O_4)_2{\cdot}2H_2O$ (a); Ti=O, NaY (not calcinated) (b); TiO_2@Y (first exchange) calcinated at 150 °C (c), anatase (d) and rutile (e). Thus, the spectrum of TiO_2@Y (c) conclusively shows the presence of anatase and rutile.

Results and discussion

Preparation and characterization of TiO_2@zeolite samples

Formation of TiO_2 clusters incorporated inside zeolites was initially accomplished using two different methodologies: either adsorption of $TiCl_4$ vapors or ion exchange using titanyl ($Ti{=}O^{2+}$) salts according to eqns. (1) and (2).

$$TiCl_4 + 2H_2 \xrightarrow{\Delta} TiO_2 + 4 \quad (1)$$

$$TiO^{2+} + H_2 \xrightarrow{\Delta} TiO_2 + 2H^+ \quad (2)$$

These two procedures lead to samples that differ substantially in the final load of TiO_2, which is much lower for the $TiCl_4$ vapor phase adsorption. TiO_2 zeolite samples prepared by $TiCl_4$ show a poorer photocatalytic performance and a detailed study of these samples was not pursued. The nomenclature and some relevant analytical and spectroscopic properties of the samples prepared are summarized in Table 1.

Formation of TiO_2 clusters by condensation of isolated Ti atoms was followed by different techniques. Oligomerization of titanium oxide is manifested in most of the physicochemical parameters of the solid and, therefore, a detailed understanding of the properties of TiO_2 clusters within zeolites requires combining information from different analytical, textural and spectroscopic techniques.

The exchange of Na^+ for $Ti{=}O^{2+}$ and the presence of $Ti{=}O^{2+}$ in the zeolites after the exchange was conveniently followed by Raman spectroscopy (Fig. 1). Thus, after ion exchange the Raman spectra of the resulting $Ti{=}O^{2+}$ exchanged zeolites show the appearance of a new intense vibrational band at *ca.* 530 cm^{-1}. This band, absent in potassium oxalate, is also observed in the potassium titanyl oxalate salt used for the ion exchange, and can be attributed to $Ti{=}O^{2+}$. The oligomerization process indicated by eqn. (2) and the condensation of TiO^{2+} into TiO_2 clusters can be assessed by Raman spectroscopy. In fact, upon mild baking of the samples at 150 °C, the Ti=O bands disappear and new vibrational bands coincident to those recorded for commercial TiO_2 anatase (394, 517 and 637 cm^{-1}), plus other bands at 460 and 810 cm^{-1}, are observed (Fig. 1).[50] The change in the Raman spectrum can be taken as spectroscopic evidence for occurrence of the oligomerization process described by eqn. (2) with formation of TiO_2 clusters.[50]

Samples of the same zeolite submitted to several consecutive $Ti{=}O^{2+}$ incorporation-oligomerization cycles were prepared (see Table 1). This procedure allows the loading of TiO_2 to be increased in each successive ion exchange until a maximum amount of TiO_2 is achieved. This amount is determined by the cavity size and by the number of exchangeable cations. Additional oligomerization could lead to the formation of adventitious TiO_2 particles not included inside the zeolite voids, which would make the material behave like bulk TiO_2 phases. The Ti content of the samples was determined by chemical analysis using X-ray fluorescence and is given in Table 1.[56] X-ray diffraction (XRD) also provided valuable information on the progress of the TiO_2 loading inside the zeolite micropores. Thus, the XRD intensity decreases during the successive $Ti{=}O^{2+}$ exchange-calcination cycles. In the case of Beta, mordenite and ZSM-5 the solids become eventually completely amorphous according to XRD data (Fig. 2). Table 1 collects the relative crystallinity for each sample compared to that of the original zeolite prior to the corresponding treatment.

Normally this loss of crystallinity is caused by damage of the zeolite framework during the manipulation of the zeolite sample either in the ion exchange or in the oligomerization of $Ti{=}O^{2+}$. Isothermal gas adsorption measurements (see Table 1)

Table 1 Relevant analytical and spectroscopic data of the TiO_2-containing zeolites

Sample	Exchange calcination cycles	Ti content/% wt	Crystallinity[a] /%	λ_{max}/nm	RD bandgap[b] /eV
TiO_2@Y	1	0.64	85	209	4.81
	2	1.29	75	210	4.77
	3[c]	1.7	68	213	4.66
TiO_2@Beta	1	4.3	52	236	3.80
	2	11.2	Amorphous	240	3.69
TiO_2@mordenite	1	0.72	85	213	4.09
	2	9.1	Amorphous	220	3.44
	3[d]	11.5	Amorphous	238	3.60
TiO_2@ZSM5	1	6.7	30	236	3.73
	2	11.7	Amorphous	240	3.44

[a] Taking the crystallinity of the original zeolite prior to the incorporation of TiO_2 clusters as 100%. [b] Measured from the interception with the x axis of the tangent at the inflexion point of the Kubelka–Munk $F(R)$ plot in the diffuse reflectance UV-Vis spectra of the samples. [c] Micropore volume 0.18 ml g^{-1}. [d] Micropore volume 0 ml g^{-1}.

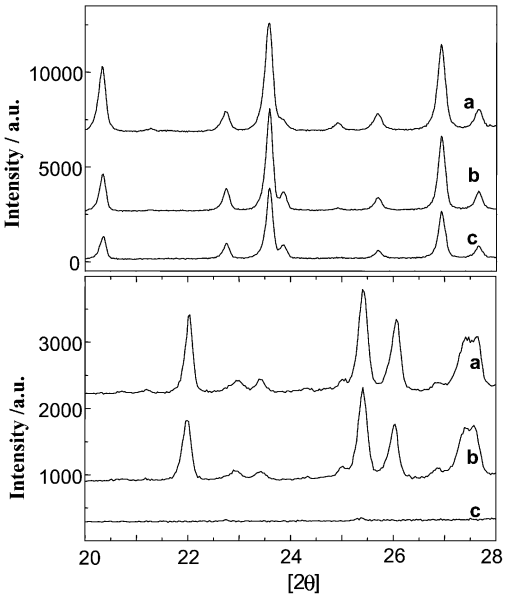

Fig. 2 X-Ray diffraction pattern of a series of zeolites. Top: pristine NaY (a) and TiO_2@Y (b: first exchange, c: third exchange). Bottom: pristine Na mordenite (a) and TiO_2@mordenite (b: first exchange, c: second exchange). For a quantitative comparison of the relative crystallinity of each sample see Table 1.

indicate that, for zeolite Y, a significant percentage of the initial pore volume of zeolite NaY (0.34 ml g^{-1}) remains after incorporation of TiO_2. In contrast, for mordenite no micropore volume is left after three consecutive $Ti{=}O^{2+}$ ion exchange cycles. Blank controls in which the zeolite samples were submitted to the same experimental procedure, but using NaCl instead of $(Ti{=}O)K_2(C_2O_4)_2{\cdot}2H_2O$ for the ion exchange, show that the final crystallinity of the Y zeolite was 78% of that of the original zeolite. The possibility that TiO_2 gradually filling the internal voids of the zeolites could contribute to a decrease in the intensity of XRD must also be considered. Since the Ti atom is heavier than Si or Al atoms, the XRD response of amorphous TiO_2 clusters may prevail over that for the crystalline zeolite host.

To address the question of the internal *vs.* external location of the TiO_2 clusters two pieces of evidence were obtained by high-resolution transmission electron microscopy (HRTEM) and XPS. HRTEM of the zeolite Y after three cycles of TiO_2 incorporation (Fig. 3) do not show the presence of observable, independent TiO_2 particles. EDX analysis of the particle shown in Fig. 3 indicates a uniform distribution of K^+ and Ti through the whole area. In contrast to TiO_2@Y, HRTEM of

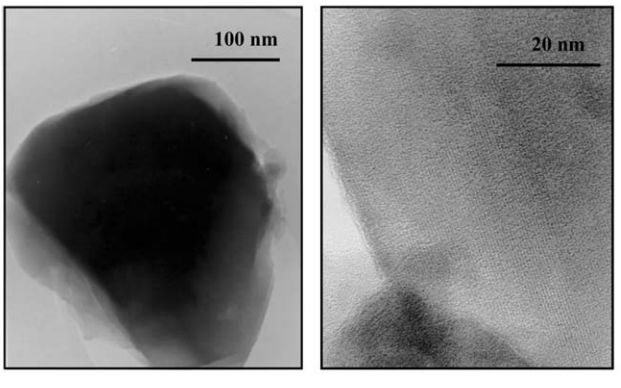

Fig. 3 Scanning electron micrograph of the TiO_2@Y sample after three consecutive $Ti{=}O^{2+}$ ion exchange oligomerization cycles. Right: enlargement of the zeolite particle shown on the left.

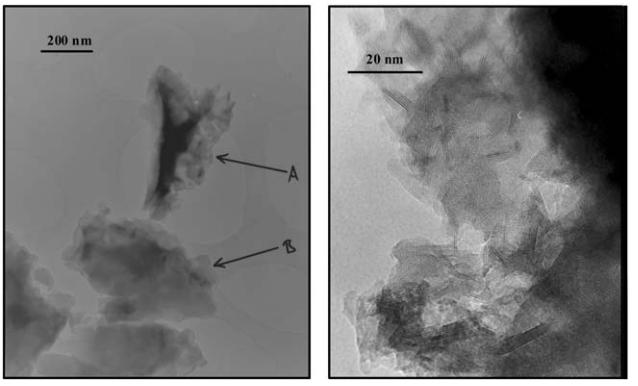

Fig. 4 Scanning electron micrograph of the TiO_2@mordenite sample prepared by three consecutive $Ti{=}O^{2+}$ ion exchange calcination cycles shows the presence of two different types of particles according to the EDX analyses. Left: Particle A has a high Ti and low Si and K content. Right: an enlargement of particle B, which has high Si and low Ti content.

TiO_2@mordenite after three ion exchange cycles shows the presence of two different type of particles in the solid (Fig. 4). One particle (labelled A in Fig. 4) has a very high Ti content and small Si and K peaks in the EDX analysis and could correspond to independent TiO_2. The second particle type (labelled B in Fig. 4) has high Si and low Ti content. Furthermore, a micrograph at higher resolution shows regular fringes characteristic of zeolite particle in particle B, but no fringes in particle A. Based on this, we suggest that TiO_2@mordenite after the third ion exchange cycle contains separated TiO_2 particles and mordenite islands. Thus, in spite of the fact that XRD of TiO_2@mordenite after the third exchange indicates that the solid has lost most of its crystallinity, some mordenite particles containing some TiO_2 have still survived the incorporation treatment and exhibit their characteristic ordering in HRTEM.

On the other hand, XPS provides a chemical analysis of the most exposed zeolite surface. By combined XPS with fast Ar^+ bombardment, which produces a partial destruction of the outermost layers, a profile of the Ti/Si atomic ratio from the exterior towards the interior of the particle can be obtained. Fig. 5 shows this profile, revealing that the actual chemical analysis of the particle is an average of the Ti distribution, which is much lower in the external surface region and increases as we penetrate into the interior of the particle. HR-TEM and XPS conclusively prove that TiO_2 clusters are formed in the interior of the zeolite Y particles or when the loading of Ti is low and the crystallinity of the zeolite high. Pore volume measurements by isothermal gas adsorption are also in agreement with the internal location of the

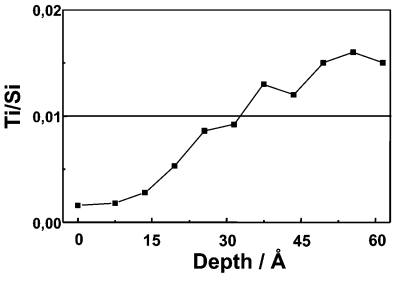

Fig. 5 Ti/Si atomic ratio as a function of the depth inside the zeolite particle obtained by XPS analysis combined with fast Ar^+ bombardment for TiO_2@mordenite (after the first ion exchange). The atomic ratio was obtained from the measurements of the Si (2p) and Ti ($2p_{3/2}$) peaks at 103.4 and 458.7 eV, respectively. The line indicates the average Ti/Si atomic ratio obtained by chemical analysis of the bulk particles.

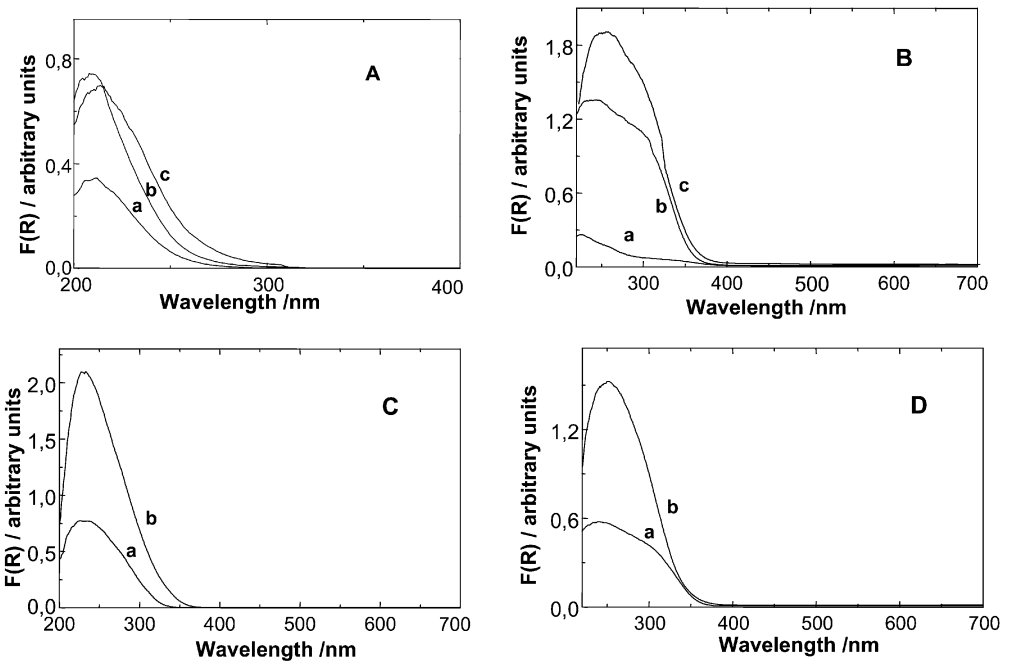

Fig. 6 DR-UVis spectra [plotted as the Kubelka–Munk function of the reflectance, $F(R)$] of TiO_2@Y (A); TiO_2@mordenite (B); TiO_2@Beta (C); and TiO_2@ZSM5 (D). The letters a, b, c correspond to samples prepared by 1, 2, 3 ion exchange cycles, respectively.

TiO_2 clusters. Thus, the initial pore volume of pristine mordenite (0.15 ml g^{-1}) is reduced to 0.10 and 0.01 ml g^{-1} for the TiO_2@mordenite samples after the first and second exchanges, respectively.

Progress of the Ti incorporation upon consecutive ion exchange cycles and formation of isolated TiO_2 particles can be conveniently followed by diffuse reflectance UV-Vis spectroscopy (DR-UV-Vis). Fig. 6 shows the DR-UV-Vis spectra of representative samples. From the optical data, it appears that in the case of large pore zeolite Y consecutive incorporation cycles gradually shift the onset of the absorbance towards longer wavelengths, indicating a dramatic influence on the semiconductor bandgap. Comparison of the DR-UV-Vis spectra of the TiO_2@Y samples with that for bulk anatase shows a remarkable increase in the bandgap for the TiO_2 cluster in zeolites, from 3.2 eV for anatase up to 4.66–4.81 eV for clusters in zeolite Y. On the other hand, the area of the absorption band increases, reflecting the increasing TiO_2 amount. Concomitantly the slope of the band also increases notably.

In addition, the presence of isolated TiO_2 particles can explain that the absorption onset for medium pore ZSM-5 and monodirectional mordenite appears at longer wavelengths than for tridirectional, large pore Y zeolite. Zeolite Beta exhibits an absorption onset intermediate between these extremes. Table 1 lists the bandgaps estimated from the DR-UV-Vis for most of the samples prepared.[50]

In the case of faujasite Y it has been proposed that the λ_{max} of the absorption band in UV-Vis diffuse reflectance can be useful to distinguish the different situations in which a monoatomic $Ti(OH)_x$ cluster can be bonded to the aluminosilicate walls. Thus, monopodally, bipodally or multipodally bonded Ti atoms have distintive λ_{max} in the optical spectrum, appearing at 278, 222 and 204 nm, respectively.[57] According to this, the spectra presented in Fig. 6(A) corresponding to TiO_2@Y would indicate that our sample contains predominantly bipodal TiO_x species.

Given the zeolite micropore dimensions in the subnanometer range in which *quantum size effects* could apply,[70] the red shift observed upon varying the zeolite structure and TiO_2 loading can be interpreted in general as reflecting an increase in the average size of the TiO_2 clusters. On the other hand, a steeper absorption band indicates a reduction in the dispersion of the cluster size with respect to a uniform distribution as the amount of TiO_2 approaches the maximum void capacity of the zeolite.

In order to support our suggestion on the operation of quantum size effects for TiO_2 clusters in the range of the pore dimensions of zeolites, we calculated at the semiempirical level the optimized geometry and HOMO–LUMO energy of a series of titanium oxides ($2 \leqslant$ number of Ti atoms $\leqslant 12$). In the models, Ti atoms were octahedrally coordinated, defining clusters of anatase structure having terminal OH groups. The charge of the clusters was set equal to zero. To save computational cost, the distance of the Ti–O bonds for the terminal ≡Ti–OH groups was fixed at a typical value of 1.95 Å. The rest of the parameters were unrestricted and geometry optimized in the calculations.

Preliminary calculations showed that the energy of the frontier orbitals of our model clusters also varies significantly depending on the connectivity of the Ti atoms and the shape of isomeric clusters having the same composition. This dependence of the HOMO–LUMO gap on the shape of the TiO_2 cluster supports our previous interpretation on the influence of the topology of the zeolite on the onset of the TiO_2 absorption band. As a general rule, our calculations show that for a given number of Ti atoms in the cluster the "linear" configurations have larger differences in the HOMO–LUMO energy than isomers having more spherical geometries. A summary of the results, including the estimated dimensions of the optimized geometry for quasi-spherical titanium oxide clusters, are collected in Table 2. In addition, Fig. 7 illustrates the optimized geometry of a cluster in the range of the zeolite Y supercage size.

The accuracy of the actual energy values given in Table 2 is limited by the level of calculation used, and by the interaction of the titanium oxide clusters with the zeolite lattice. Thus, obviously the values obtained are only meaningful to show a trend in the frontier orbitals of the series. From these data, it appears that the number of Ti atoms has a large initial effect that tends to level off, even for clusters containing a relatively small number of Ti atoms.

Table 2 Frontier orbital energy values and cluster dimensions as a function of the number of Ti atoms for TiO_2 clusters, calculated by semiempirical methods

Number of Ti atoms	HOMO energy/eV	LUMO energy/eV	Dimensions of the cluster/Å × Å
2	−9.273	−1.471	7.88 × 4.45
3	−8.875	−1.717	7.60 × 7.43
5	−8.531	−2.634	9.37 × 6.81
6	−8.158	−2.856	14.01 × 7.74
7	−8.704	−2.225	10.73 × 7.93
8	−8.378	−2.466	13.82 × 7.93
9	−8.782	−4.053	14.71 × 9.10
10	−8.310	−5.527	14.64 × 10.01
12	−8.104	−6.338	15.52 × 12.04

Photocatalytic activity

An exploratory study aimed at determining the photocatalytic activity of these TiO_2@zeolite samples compared to standard TiO_2 anatase was carried out. We chose for this study the photocatalytic oxygenation of an electron-rich heterocycle in aerated dichloromethane and the photocatalytic deactivation of an enzyme in aqueous medium. The selection of these two very different TiO_2 activated processes was based on previous literature work on the use of TiO_2, and in an attempt to cover two general photocatalytic processes promoted by TiO_2 involving the intermediacy of organic radical cations or hydroxyl radicals, respectively. These two photocatalytic processes take place under totally different experimental conditions and thus provide a measure of the usefulness of tuning the catalytic properties of TiO_2 by inclusion in zeolites.

Concerning the photooxidation of thianthrene in dichloromethane, there are numerous reports showing the ability of TiO_2 to promote photooxygenations of electron-rich aromatic, alkylaromatic and olefinic compounds in organic solvents.[71–73] In some cases the mechanism has been shown to involve the reaction of photogenerated organic radical cations with molecular oxygen. Alternatively, the chlorinated solvent may trap photogenerated electrons and holes, giving rise to a radical mechanism that can also lead to photooxygenation products.

In the present study we have compared the activity of some TiO_2@zeolite samples with that of standard TiO_2 anatase for thianthrene photooxygenation (Scheme 1). The major product observed was thianthrene oxide, with occasionally minor amounts of thianthrene dioxide. The results are included in Table 3.

Given that the TiO_2@zeolite samples have their absorption maxima shifted to shorter wavelengths compared to commercial TiO_2, no appreciable photoreaction was observed using

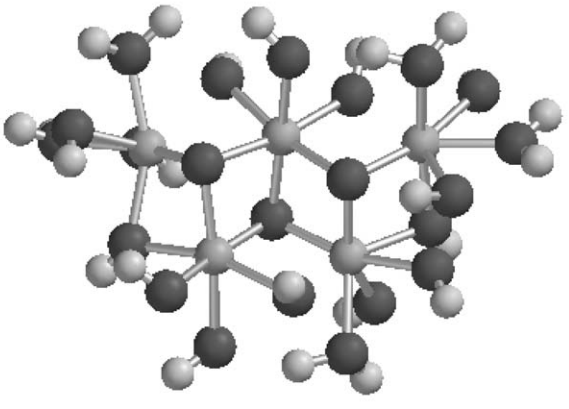

Fig. 7 Molecular modelling of a $(TiO_2)_5$ cluster based on a quantum mechanical semiempirical method.

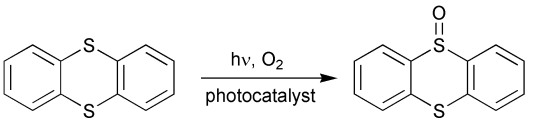

Scheme 1

TiO_2@zeolite photocatalysts when the irradiation was carried out through pyrex. In contrast, standard TiO_2 solid exhibits a similar activity for the photooxygenation either in pyrex or quartz. Since pyrex acts as an efficient cut-off filter for wavelengths shorter than 300 nm,[74] this observation is in agreement with the DR-UV-Vis spectrum of anatase having significant absorption at longer wavelengths than the TiO_2@zeolite samples.

However, when working in quartz containers, and using germicidal lamps (rich in 254 nm light) as the excitation source, the activity of the TiO_2@zeolite improves remarkably, surpassing the results of the photochemical TH oxygenation in the absence or presence of P-25 TiO_2 standard (see Table 3). Thus, it seems that the apparent photoactivity of TiO_2 clusters within zeolites in terms of substrate conversion can be even higher than that of a TiO_2 standard.[75,76] Under these irradiation conditions a certain level of direct thianthrene excitation is unavoidable. Parallel blank controls in the absence of any solid photocatalyst led to the formation of some thianthrene oxide (see Table 3), although its yield was significantly lower than in the presence of TiO_2 containing zeolite. Related precedents in which the excitation source and conditions for TiO_2 photocatalysis may also result in the direct excitation of the substrate can be found in the literature.[72] Although the similar photoactivity of TiO_2@Y and TiO_2@mordenite do not reflect differences in TiO_2 loading and bandgap, this can be due to the fact that under the experimental conditions employed there is a large excess of photocatalyst.

Besides irradiation in organic solvents, TiO_2 photocatalysis in aqueous solution has attracted considerable interest.[6] It is assumed that the general reaction mechanism in aqueous media involves predominantly the generation of highly reactive hydroxyl radicals. Other active oxygen species can also be generated and intervene in the photooxidation mechanism under these conditions. The primary active oxygen species, particularly $^{\bullet}OH$ radicals,[5,77–81] attack any organic solute present in the water, initiating its oxidative degradation. In the absence of any species susceptible to be attacked by $^{\bullet}OH$, the photocatalytic irradiation in water may result in the formation of a stationary concentration of hydrogen peroxide.[82] In fact, we have been able to detect the formation of a photostationary 1.8 mM concentration of H_2O_2 in the 254 nm irradiation of distilled water through quartz in the presence of TiO_2@Y. In contrast, analogous photoirradiation using the standard TiO_2 anatase does not lead to a measurable photostationary concentration of H_2O_2. At 254 nm H_2O_2 undergoes a slow photochemical degradation and the photostationary concentration using TiO_2@Y as photocatalyst implies that the formation and

Table 3 Results of the direct and photocatalyzed TH oxygenation upon 254 nm UV lamp irradiation

	Yield of TH=O/%	
Photocatalyst	1 h	5 h
None	5	26
NaY	2	15
TiO_2@Y (first exchange)	22	74
TiO_2@mordenite (first exchange)	21	62
P-25 TiO_2	4	24

decomposition rates of H_2O_2 under these conditions and at this concentration are the same.

We have also considered the effect the irradiation of TiO_2@-zeolite would have when in the presence of susceptible biological substrates in aqueous media. This is of relevance in the context of the widespread use of TiO_2 in sunscreens and cosmetics. The photocatalytic activity of TiO_2 has been studied in relation to biologically relevant substrates in aqueous solution. Studies with amino acids and nucleic acids have shown that irradiation with UVA light in the presence of TiO_2 catalyzes the degradation of these biomolecules.[83–91]

An earlier study from our group has shown that TiO_2 particles in aqueous suspension efficiently inactivate horseradish peroxidase (HRP),[92] a heme enzyme that decomposes H_2O_2 in the presence of a suitable substrate. HRP belongs to a large family of peroxidases widely distributed in nature. While HRP is not found in humans, many other peroxidases are. Photoinduced inactivation of HRP by TiO_2 occurs under both anaerobic and aerobic conditions, but it is far more effective under the latter conditions. The process consequently occurs with the destruction of the heme group, which is the catalytic center in these enzymes. It is possible that while damage is the worst on the heme group, reactions also occur at the protein frame.

We have thus studied the photocatalytic behavior of TiO_2 when included in zeolites Y and mordenite, in aqueous solution containing HRP as a test biological substrate. Broadband irradiation of the solutions was performed around 350 nm, to avoid direct absorption of light by the protein. Following irradiation, the activity of the HRP enzyme was analyzed in the presence of the substrate, 2,2′-azinobis(3-ethylbenzthiazoline-6-sulfonic acid) diammonium salt (ABTS). In order to compare the activity of TiO_2@zeolite with that of anatase TiO_2, the irradiations were performed under the same conditions for both species. Control experiments were done with HRP samples irradiated without photocatalyst and unexposed samples in the presence of TiO_2 anatase, TiO_2@zeolite, or free of any catalyst.

Our results (see Table 4 and Fig. 8) show that in contrast to thianthrene photooxidation, the photocatalytic activity of the TiO_2 anatase is higher than that of TiO_2@zeolite in the case of enzyme photoinactivation. Note also that the activity of TiO_2@Y is lower than that of TiO_2@mordenite. As already discussed (*vide supra*) the TiO_2@zeolite absorption is blue-shifted relative to TiO_2 anatase, and therefore exhibits lower activity under 350 nm irradiation. The same argument explains why the activity of TiO_2@mordenite is higher than that of TiO_2@Y. The absorption threshold for the latter is less extended into the UVA region of the spectrum as compared to the former (see Fig. 6).

In summary, by encapsulation within the zeolite voids we have been able to alter the photochemical activity of TiO_2. This photoactivity is different from that of bulk P-25 anatase and varies depending on the zeolite framework and TiO_2 loading. In this way we have prepared TiO_2 containing photocatalysts that are more active than pure TiO_2 for thianthrene photooxygenation and less active than pure TiO_2 for enzyme photoinactivation. In both cases, this is the desirable effect on the photocatalytic activity of TiO_2. In addition, our methodology can be used to develop more elaborated multicomponent photocatalytic systems containing nanometric TiO_2 clusters as one of the constituents.[63,64]

Table 4 Relative enzymatic activity measured for HRP in water and in the presence of different photocatalysts. Results are an average of three measurements. Activity values were obtained from coefficient *b* of the fitting curve for each sample (see Fig. 8) and then normalized to the value presented for the dark sample in each case to obtain the relative values. Dark samples exhibited an activity value of 0.15 units of absorbance change at 412 nm per second per 41 ng ml^{-1} of enzyme

Sample	Relative enzymatic activity/%
HRP	100
HRP + TiO_2@Y (first exchange)	81
HRP + TiO_2@mordenite (first exchange)	65
HRP + TiO_2 anatase	2

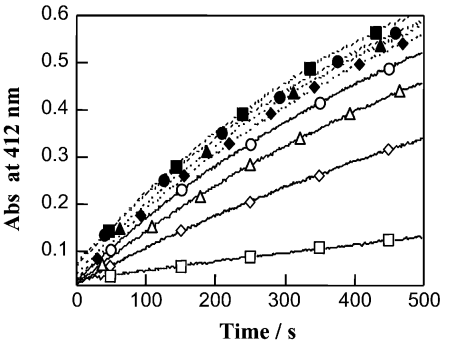

Fig. 8 HRP catalyzed oxidation of ABTS as a function of time. The HRP activity is given by the slope of the curves. ● HRP non-irradiated, ○ HRP irradiated, ▲ HRP non-irradiated in the presence of TiO_2@Y (first exchange). △ HRP irradiated in the presence of TiO_2@Y (first exchange). ◆ HRP non-irradiated in the presence of TiO_2@mordenite (first exchange), ◇ HRP irradiated in the presence of TiO_2@mordenite (first exchange), ■ HRP non-irradiated in the presence of TiO_2 anatase. □ HRP irradiated in the presence of TiO_2 anatase.

Experimental

TiO_2@zeolite preparation and characterization

The corresponding zeolite in its Na^+ form (10 g) was stirred at room temperature with a solution of $(Ti{=}O)K_2(C_2O_4)_2{\cdot}2H_2O$ or $(NH_4)_2(Ti{=}O)(C_2O_4)_2{\cdot}H_2O$ at the required concentration (0.05, 0.4 and 0.8 M) for 4 h. After this time, the solid was filtered and washed exhaustively with distilled water until no oxalate anions were detectable in the washing waters using a freshly prepared 0.5 M aqueous solution of $CaCl_2$. The solids were dried in an oven at 150 °C for 5 h. Alternatively, TiO_2 was incorporated by submitting the zeolite sample (1 g) placed in a tubular reactor to a stream of dry nitrogen that had been bubbled through liquid $TiCl_4$ at room temperature. The system allows the *in situ* partial dehydration of the zeolite prior to the $TiCl_4$ treatment by heating the tubular reactor at temperatures between 100 and 300 °C for 1 h prior to passing the $TiCl_4$ vapors.

The elemental analyses were carried out by X-ray fluorescence spectroscopy using a Phillips MiniPal 25 fm. Powder X-ray diffractions were recorded with a Philips X'Pert PW3719 diffractometer equipped with a graphite polarizer, automatic slits with a total scan surface of 14 mm and a proportional detector. The diffractometer operates with Cu K_α radiation working at an excitation power of 2 kW; the goniometer angular speed was 0.02° s^{-1}. High-resolution transmission electron micrographs and EDX analysis were recorded at the University of Reading with a Philips CM20 instrument. Micropore volumes were obtained by isothermal N_2 adsorption in a Micromeritics apparatus. XPS measurements were carried out at room temperature with a concentric hemispherical analyzer operated in the constant pass energy mode (50 eV). A Mg Kα X-ray source ($h\nu = 1253.6$ eV) was used. A vacuum of *ca.* 5×10^{-9} Torr was always attained in the analysis chamber during XPS recording. Charging effects were calibrated by the C (1s) line at 284.6 eV. Diffuse reflectance UV-Vis spectra were recorded in a Cary 5G spectrophotometer using a praying mantis accessory and $BaSO_4$ as reference. Laser Raman

spectra were recorded on a Bio-Rad spectrometer, Model FT-Raman II. The 1.064 μm line of a Nd : YAG laser was used for excitation along with a Ge detector cooled to liquid nitrogen temperature. Samples were examined in the 180° scattering configuration using high-quality quartz tubes as cells. The laser power at the samples was *ca.* 120 mW. The Raman spectra were corrected for instrumental response using a white light reference spectrum. Quantum chemical calculations were carried out at the semiempirical level using the PM3 method implemented in the Spartan Pro program.

Thianthrene photooxygenation

Titanium dioxide, pure anatase, with an average particle size of 32 nm was purchased from Degussa P-25. Suspensions of thianthrene (50 mg, Aldrich used as received) in dichloromethane (20 ml) containing the required photocatalyst (150 mg) were simultaneously irradiated (open to ambient air) at room temperature under magnetic stirring under air for 4 h. Low pressure mercury lamps of 254 and 300 nm were used as excitation sources and the sample contained in quartz or pyrex glassware, respectively. The course of the photoreaction was periodically followed by analyzing filtered aliquots by GC (Varian, 25 m 5% crosslinked phenyl methyl silicone with a FID) or GC-MS using *n*-decane as the external standard for calibration. Characterization of the photoproducts was accomplished by comparing the reaction time and MS with authentic specimens prepared according to reported procedures.[93,94]

H_2O_2 titrations

A suspension of the corresponding photocatalyst in distilled water was photolyzed in air under magnetic stirring at 254 nm through quartz. Filtered aliquots were iodimetrically titrated and the result corrected by subtracting a blank irradiated under the same conditions but in the absence of any photocatalyst.

Horseradish peroxidase inactivation

Horseradish peroxidase (HRP), type VI-A and 2,2′-azinobis(3-ethylbenzthiazoline-6-sulfonic acid)diammonium salt (ABTS), were purchased from Sigma and used as received. All buffers were prepared using filtered millipore water (Millipore Milli-Q system) and reagent grade chemicals. All buffers were treated with a chelating resin, iminodiacetic acid (from Sigma), to remove any metal ions.

Steady state photolyses were performed using an irradiation chamber fitted with 350 nm Rayonet UVA lamps. Samples containing only HRP (0.025 mg mL^{-1}) as well as those containing both enzyme and TiO_2@zeolite (0.25 mg mL^{-1}) or enzyme and TiO_2 anatase (0.025 mg mL^{-1}) in a 4 ml volume, were photolyzed in pyrex test tubes (1 cm i.d., 5 mL total volume). Dark control samples were placed in the chamber to ensure that all samples (exposed and unexposed ones) were kept under the same conditions. HRP activity assays were performed with [ABTS] = 0.025 mM and [H_2O_2] = 0.25 mM, prepared in a buffer of pH 4.4. The choice of this pH was dictated by the assay procedure, which reflects the pH at which the enzyme exhibits significant activity. To 5 ml of the solution of ABTS and H_2O_2 a diluted fraction, ~5 ng, of the enzyme was added (HRP solutions were diluted 1/4500 for the assay) according to the assay procedure of Porstmann *et al.*[95] All activity assays were monitored at 412 nm using a Milton-Roy 3000, UV-visible spectrophotometer in kinetics mode. Absorption spectra were acquired on the same instrument used in scan mode. Plots of kinetic data were constructed using Kaleidagraph software and fitted with a second-order polynomial equation to determine the initial slopes. Each curve is then fitted with the expression[92] $A_{412\ nm} = a + bt + ct^2$, where A is the absorbance and t the time. The coefficients *a, b* and *c* are fitting parameters. The derivative of this expression with respect to t is given by $dA_{412}/dt = b + 2ct$, which at $t = 0$ corresponds to b. That is, the first coefficient (b) of the quadratic fit is the calculated initial slope. These slopes have been used as a measure of the enzymatic activity.

Acknowledgements

Financial support by the Spanish DGICYT (HG, MAT2000-1768-C02-01) and NSERC (Canada) through an operating grant (JCS) is gratefully acknowledged. GC thanks the Ontario Graduate Scholarship Program for a postgraduate scholarship. LF also thanks the Spanish Ministry of Education for a fellowship. We are grateful to Dr. Tanya Hancock-Chen for her help with the enzyme work and Dr. Peter Harris (University of Reading) for providing the high resolution electron microscopy shown in Figs. 3 and 4.

References

1 M. Anpo, H. Yamashita, K. Ikeue, Y. Fujii, S. G. Zhang, Y. Ichihashi, D. R. Park, Y. Suzuki, K. Koyano and T. Tatsumi, *Catal. Today*, 1998, **44**, 327.
2 M. Anpo, Y. Ichihashi, M. Takeuchi and H. Yamashita, *Res. Chem. Intermed.*, 1998, **24**, 143.
3 J. R. Bolton, K. G. Bircher, W. Tumas and C. A. J. H. Tolman, *Adv. Oxid. Technol.*, 1996, **1**, 13.
4 H. Kominami, S. Murakami, Y. Kera and B. Ohtani, *Catal. Lett.*, 1998, **56**, 125.
5 D. F. Ollis and H. Al-Ekabi, *Photocatalytic Purification and Treatment of Water and Air*, Elsevier, Amsterdam, 1993.
6 O. Legrini, E. Oliveros and A. M. Braun, *Chem. Rev.*, 1993, **93**, 671.
7 M. I. Cabrera, A. C. Negro, O. M. Alfano and A. E. Cassano, *J. Catal.*, 1997, **172**, 386.
8 L. Cermenati, A. Albini, P. Pichat and C. Guillard, *Res. Chem. Intermed.*, 2000, **26**, 221.
9 J. Chen, D. F. Ollis, W. H. Rulkens and H. Bruning, *Water Res.*, 1999, **33**, 1173.
10 J. Chen, D. F. Ollis, W. H. Rulkens and H. Bruning, *Water Res.*, 1999, **33**, 661.
11 J. Chen, D. F. Ollis, W. H. Rulkens and H. Bruning, *Water Res.*, 1999, **33**, 669.
12 Q. Dai, N. Y. He, K. P. Weng, B. P. Lin, Z. H. Lu and C. W. Yuan, *J. Inclusion Phenom. Mol. Recognit. Chem.*, 1999, **35**, 11.
13 Q. Dai, Z. L. Zhang, N. Y. He, P. Li and C. W. Yuan, *Mater. Sci. Eng., C*, 1999, 417.
14 X. J. Li, J. W. Cubbage, T. A. Tetzlaff and W. S. Jenks, *J. Org. Chem.*, 1999, **64**, 8509.
15 X. J. Li, J. W. Cubbage and W. S. Jenks, *J. Org. Chem.*, 1999, **64**, 8525.
16 M. I. Litter, *Appl. Catal., B*, 1999, **23**, 89.
17 V. Loddo, G. Marci, L. Palmisano and A. Sclafani, *Mater. Chem. Phys.*, 1998, **53**, 217.
18 S. Malato, J. Blanco, C. Richter and M. I. Maldonado, *Appl. Catal., B*, 2000, **25**, 31.
19 K. T. Ranjit, I. Willner, S. Bossmann and A. Braun, *J. Phys. Chem. B*, 1998, **102**, 9397.
20 M. R. Dhananjeyan, J. Kiwi and K. R. Thampi, *Chem. Commun.*, 2000, 1443.
21 M. A. Malati, *Environ. Technol.*, 1995, **16**, 1093.
22 G. A. Penuela and D. Barcelo, *Trends Anal. Chem.*, 1998, **17**, 605.
23 T. E. Mallouk, E. H. Yonemoto, R. L. Riley, Y. I. Kim, S. J. Atherton and R. H. Schmehl, *J. Am. Chem. Soc.*, 1992, **114**, 8081.
24 A. Kudo, H. Kato and S. Nakagawa, *J. Phys. Chem. B*, 2000, **104**, 571.
25 A. Kudo, K. Domen, K. Maruya and T. Onishi, *Chem. Phys. Lett.*, 1987, **133**, 517.
26 K. Sayama and H. Arakawa, *J. Chem. Soc., Faraday Trans.*, 1997, **93**, 1647.
27 A. Hagfeldt and M. Gratzel, *Acc. Chem. Res.*, 2000, **33**, 269.
28 D. Cahen, G. Hodes, M. Grätzel, J. F. Guillemoles and I. Riess, *J. Phys. Chem. B*, 2000, **104**, 2053.
29 B. O'Regan and M. Grätzel, *Nature*, 1991, **335**, 737.

30 M. K. Nazeeruddin, A. Kay, I. Rodicio, R. Humphry-Baker, E. Müller, P. Liska, N. Vlachopoulos and M. Grätzel, *J. Am. Chem. Soc.*, 1993, **115**, 6382.
31 R. Amadelli, R. Argazzi, C. A. Bignozzi and F. Scandola, *J. Am. Chem. Soc*, 1990, **112**, 7029.
32 M. Alebbi, C. A. Bignozzi, T. A. Heimer, G. Hasselmann and G. J. Meyer, *J. Phys. Chem. B*, 1998, **102**, 7577.
33 M. K. Nazeeruddin, P. Péchy and M. Grätzel, *Chem. Commun.*, 1997, 1705.
34 A. Islam, H. Sugihara, K. Hara, L. P. Singh, R. Katoh, M. Yanagida, Y. Takahashi, S. Murata and H. Arakawa, *New J. Chem.*, 2000, **24**, 343.
35 N.-G. Park, G. Schlichthörl, J. van de Lagemaat, H. M. Cheong, A. Mascarenhas and A. J. Frank, *J. Phys. Chem. B*, 1999, **103**, 3308.
36 K. Kalyanasundaram and M. Gratzel, *Proc. Indian Acad. Sci., Chem. Sci.*, 1997, **109**, 447.
37 Y. Liu and R. O. Claus, *J. Am. Chem. Soc.*, 1997, **119**, 5273.
38 C. Kormann, D. W. Bahnemann and M. R. Hoffmann, *J. Phys. Chem.*, 1988, **92**, 5196.
39 S. Logunov, T. Green, S. Marguet and M. A. El-Sayed, *J. Phys. Chem. A*, 1998, **102**, 5652.
40 W. Choi, A. Termin and M. R. Hoffmann, *J. Phys. Chem.*, 1994, **98**, 13 669.
41 N. Serpone, D. Lawless and R. Khairutdinov, *J. Phys. Chem.*, 1995, **99**, 16 646.
42 S. Monticone, R. Tufeu and A. V. Kanaev, *Chem. Phys. Lett.*, 1998, **294**, 237.
43 Z. B. Zhang, C. C. Wang, R. Zakaria and J. Y. Ying, *J. Phys. Chem. B*, 1998, **102**, 10 871.
44 T. Matsumoto, Y. Murakami and Y. Takasu, *J. Phys. Chem. B*, 2000, **104**, 1916.
45 S. T. Martin, C. L. Morrison and M. R. Hoffmann, *J. Phys. Chem.*, 1994, **98**, 13 695.
46 H. Yamashita, Y. Ichihashi, M. Anpo, M. Hashimoto, C. Louis and M. Che, *J. Phys. Chem.*, 1996, **100**, 16 041.
47 H. Yamashita, Y. Fujii, Y. Ichihashi, S. G. Zhang, K. Ikeue, D. R. Park, K. Koyano, T. Tatsumi and M. Anpo, *Catal. Today*, 1998, **45**, 221.
48 Y. Xu and C. H. Langford, *J. Phys. Chem. B*, 1997, **101**, 3115.
49 Y. Xu and C. H. Langford, *J. Phys. Chem.*, 1995, **99**, 11 501.
50 X. Liu, K.-K. Iu and J. K. Thomas, *J. Chem. Soc., Faraday Trans.*, 1993, **89**, 1861.
51 Y. I. Kim, S. W. Keller, J. S. Krueger, E. H. Yonemoto, G. B. Saupe and T. E. Mallouk, *J. Phys. Chem. B*, 1997, **101**, 2491.
52 M. A. Fox, K. E. Doan and M. T. Dulay, *Res. Chem. Intermed.*, 1994, **20**, 711.
53 M. Anpo, H. Yamashita, Y. Ichihashi, Y. Fujii and M. Honda, *J. Phys. Chem. B*, 1997, **101**, 2632.
54 S. H. Bossmann, D. Herrmann, A. M. Braun and C. Turro, *J. Inf. Rec.*, 1998, **24**, 271.
55 M. Anpo, H. Yamashita, M. Matsuoka, D. R. Park, Y. G. Shul and S. E. Park, *J. Ind. Eng. Chem.*, 2000, **6**, 133.
56 G. Grubert, M. Wark, N. I. Jaeger, G. Schulz-Ekloff and O. P. Tkachenko, *J. Phys. Chem. B*, 1998, **102**, 1665.
57 J. Klaas, G. Schulz-Ekloff and N. I. Jaeger, *J. Phys. Chem B*, 1997, **101**, 1305.
58 M. Wark, H. J. Schwenn, N. I. Jaeger and B. Boddenberg, *Stud. Surf. Sci. Catal.*, 1995, **97**, 205.
59 M. Wark, M. Koch, A. Brückner and W. Grünert, *J. Chem. Soc., Faraday Trans.*, 1998, **94**, 2033.
60 R. M. Barrer, *Zeolites and Clay Minerals as Sorbents and Molecular Sieves*, Academic Press, London, 1978.
61 D. W. Breck, *Zeolite Molecular Sieves: Structure, Chemistry and Use*, John Wiley and Sons, London, 1974.
62 H. van Bekkum, E. M. Flanigen and J. C. Jansen, *Introduction to Zeolite Science and Practice*, Elsevier, Amsterdam, 1991.
63 G. Cosa, M. Chrétien, M. S. Galletero, V. Fornés, H. García and J. C. Scaiano, *J. Phys. Chem. B*, 2002, **106**, 2460.
64 S. H. Bossmann, C. Turro, C. Schnabel, M. R. Pokhrel, K. Janik and M. Wörner, *J. Phys. Chem. B*, 2001, **105**, 5374.
65 S. Corrent, G. Cosa, J. C. Scaiano, M. S. Galletero, M. Alvaro and H. García, *Chem. Mater.*, 2001, **13**, 715.
66 Y. Paz and A. Heller, *J. Mater. Res.*, 1997, **12**, 2759.
67 Y. Paz, Z. Luo, L. Rabenberg and A. Heller, *J. Mater. Res.*, 1995, **10**, 2842.
68 A. Heller, Y. Degani, D. W. Johnson, Jr. and P. K. Gallagher, *Proc. -Electrochem. Soc.*, 1988, **88**, 23.
69 A. Heller, Y. Degani, D. W. Johnson, Jr. and P. K. Gallagher, *J. Phys. Chem.*, 1987, **91**, 5987.
70 R. Rossetti, J. L. Ellison, J. M. Gibson and L. E. Brus, *J. Chem. Phys.*, 1984, **80**, 4464.
71 M. A. Fox and M. Chanon, in *Photoinduced Electron Transfer, Part C*, Elsevier, Amsterdam, 1988.
72 M. A. Fox and M. T. Dulay, *Chem. Rev.*, 1993, **93**, 341.
73 M. A. Fox, in *Photocatalysis—Fundamentals and Applications*, ed. N. Serpone and E. Pellizzetti, Wiley Interscience, New York, 1989, p. 421.
74 S. L. Murov, *Handbook of Organic Photochemistry*, Marcel Dekker, New York, 1973.
75 The absolute efficiency of each material should take into account the photons actually adsorbed by each material instead the emitted photons and cannot be calculated. See also next reference.
76 N. Serpone and A. Salinaro, *Pure Appl. Chem.*, 1999, **71**, 303.
77 Y. Nosaka, Y. Yamashita and H. Fukuyama, *J. Phys. Chem. B*, 1997, **101**, 5822.
78 P. F. Schwarz, N. J. Turro, S. H. Bossmann, A. M. Braun, A.-M. A. A. Wahab and H. Dürr, *J. Phys. Chem. B*, 1997, **101**, 7127.
79 B. Kraeutler and A. J. Bard, *J. Am. Chem. Soc.*, 1978, **100**, 2239.
80 L. Cermenati, P. Pichat, C. Guillard and A. Albini, *J. Phys. Chem. B*, 1997, **101**, 2650.
81 S. N. Frank and A. J. Bard, *J. Phys. Chem.*, 1977, **81**, 1484.
82 T. Wu, G. Liu, J. Zhao, H. Hidaka and N. Serpone, *J. Phys. Chem. B*, 1999, **103**, 4862.
83 M. R. Dhananjeyan, R. Annapoorani and R. Renganathan, *J. Photochem. Photobiol. A*, 1997, **109**, 147.
84 H. Hidaka, S. Horikoshi, K. Ajisaka, J. Zhao and N. Serpone, *J. Photochem. Photobiol. A*, 1997, **108**, 197.
85 H. Hidaka, T. Shimura, K. Ajisaka, S. Horikoshi, J. C. Zhao and N. Serpone, *J. Photochem. Photobiol. A*, 1997, **109**, 165.
86 S. Horikoshi, N. Serpone, J. C. Zhao and H. Hidaka, *J. Photochem. Photobiol. A*, 1998, **118**, 123.
87 S. Horikoshi, N. Serpone, S. Yoshizawa, J. Knowland and H. Hidaka, *J. Photochem. Photobiol. A*, 1999, **120**, 63.
88 H. Hidaka, K. Ajisaka, S. Horikoshi, T. Oyama, J. C. Zhao and N. Serpone, *Catal. Lett.*, 1999, **60**, 95.
89 H. Hidaka, S. Horikoshi, N. Serpone and J. Knowland, *J. Photochem. Photobiol. A*, 1998, **111**, 205.
90 W. G. Wamer, J. J. Yin and R. R. Wei, *Free Radical Biol. Med.*, 1997, **23**, 851.
91 R. Dunford, A. Salinaro, L. Z. Cai, N. Serpone, S. Horikoshi, H. Hidaka and J. Knowland, *FEBS Lett.*, 1997, **418**, 87.
92 T. Hancock-Chen and J. Scaiano, *J. Photochem. Photobiol. B*, 2000, **57**, 193.
93 W. Adam and D. Golsch, *Chem. Ber.*, 1994, **127**, 1111.
94 W. Adam, D. Golsch and F. C. Goerth, *Chem. Eur. J.*, 1996, **2**, 255.
95 B. Porstmann, T. Porstmann and M. Nugel, *J. Clin. Chem. Biochem.*, 1981, **19**, 435.